Strain Rate Effect on Mechanical Behaviors of Nylon 6–Clay Nanocomposites

Jia-Lin Tsai and Jen-Chieh Huang

Journal of Composite Materials 2006 40: 925
DOI: 10.1177/0021998305056382

Strain Rate Effect on Mechanical Behaviors of Nylon 6–Clay Nanocomposites

JIA-LIN TSAI* AND JEN-CHIEH HUANG
Department of Mechanical Engineering
National Chiao Tung University
Hsinchu, Taiwan 300

(Received October 12, 2004)
(Accepted May 9, 2005)

ABSTRACT: This study aims to investigate strain rate effect on the mechanical behaviors of nylon 6–clay nanocomposites. Both dry and wet nylon 6–clay nanocomposites are examined in this study. To determine the strain rate effect, the nylon 6 nanocomposites with 5 wt% loading of the organoclay are tested in compression at different strain rates. For strain rates less than 1/s, the experiments are conducted using a hydraulic MTS machine. However, the high strain rate tests are performed using a split Hopkinson pressure bar (SHPB). To establish reliable dynamic stress and strain curves for the nanocomposites, a pulse-shaper technology is employed in the SHPB tests. Experimental observations reveal that for dry nanocomposites, the linear portions of the stress and strain curves are not affected substantially by the strain rates, but the yielding stresses increase with the increment of the strain rates. On the other hand, for the wet nanocomposites, the stress and strain curves are almost nonlinear demonstrating significant stiffening behaviors as the strain rates increase. This stiffening behavior is continuous until the stress and strain curves are almost linear at the strain rate of 500/s. Comparison of nylon 6–clay nanocomposites and unfilled nylon 6 indicates that the supplement of 5 wt% organoclay in the dry nylon 6 can enhance the Young's modulus to 32% within the tested strain rate ranges. Moreover, for the wet nylon reinforced with organoclay, the increment of Young's modulus can be achieved up to 43%.

KEY WORDS: split Hopkinson pressure bar, nylon 6, nanocomposites, strain rate effect, moisture effect.

INTRODUCTION

COMPOSITES REINFORCED WITH nanoclay platelets have been of great interest to many researchers [1], with the latest developments in nanotechnology. The nanoclay platelet is an ultrathin (1 nm) silicate film with lateral dimensions up to 1 μm. Without special processing, the platelets are held together by weak ionic bonds into clay tactoids. Through

*Author to whom correspondence should be addressed. E-mail: jialin@mail.nctu.edu.tw

0021-9983/06/10 0925–14 $10.00/0 DOI: 10.1177/0021998305056382

the ion exchange process, the sodium ions on the surfaces of the platelets are replaced with organic cations, which can improve the interfacial adhesion between the polymer and the platelet. After an appropriate process, such as polymerization [2] and melt compounding [3], the aggregated platelets can be exfoliated and uniformly dispersed in the polymer. Depending on the degree of exfoliation, three categories of nanocomposites are generated, i.e., tactoid, intercalated, and exfoliated [4]. Toyota research center carried out a pioneering study on synthesizing nylon 6–clay nanocomposites using the polymerization process. The increments of tensile strength, modulus, and heat distortion temperature relative to pure resin were reported in [5,6]. Cho and Paul [3] demonstrated the preparation of nylon 6–organoclay nanocomposites through the direct melt compounding process using a conventional twin-screw extruder. They found that the relative stiffness and strength of the materials prepared by melt compounding were quite comparable with those of the nanocomposites formed by *in situ* polymerization. A similar process for the fabrication of nanocomposites using a twin-screw extruder was employed by Liu et al. [7]. They found that the nanocomposites were superior to nylon 6 in terms of strength and modulus. Tsai and Sun [8] developed an analytical approach on the load transfer efficiency of organoclay platelets in a polymer matrix using a shear lag model with an appropriate representative volume element (RVE). They demonstrated that well dispersed and exfoliated platelets in the polymer matrix could significantly enhance the load transfer efficiency. It is to be noted that in the above studies, the experimental results of nanocomposites were obtained based on quasi-static tests.

However, polymeric materials, in general, exhibit strain rate sensitivity when subjected to dynamic loading [9,10]. The high strain rate properties of the polymers, Epon 828–T-403 and PMMA, were characterized by Chen et al. [9] using a split Hopkinson pressure bar (SHPB) and higher compressive strengths were observed in their dynamic compression tests. The experimental results for a variety of polymers at different strain rates can be found in Walley et al. [10]. Due to the rate-dependent characteristic of the polymeric material, the associated mechanical behaviors of the polymer-based nanocomposite may alter in accordance with different loading rates. However, so far, only few studies concerning the strain rate effect on the organoclay–polymer nanocomposites were reported.

The objective of this study is to conduct systematic investigation on the rate-dependent behaviors of nylon 6–clay nanocomposites. To demonstrate the strain rate effect, the nanocomposite samples were tested in compression at different strain rates. For low strain rates, the experiments were conducted on an MTS machine, while the high strain rate tests were performed using the SHPB. Based on the experimental data, the constitutive relations of the nanocomposites at various strain rates were generated and from which, the Young's modulus were determined. In addition, for comparison, unfilled nylon 6 was tested in the same manner and the effects of the organoclay on the mechanical responses of the nanocomposites were addressed.

SPECIMEN PREPARATION

The nylon 6–clay nanocomposites (RTP 299AX) and unfilled nylon 6 (RTP 200A) in the form of pellets are available commercially from RTP Company, USA. According to the information provided by the manufacturer, the nanocomposite pellets containing 5 wt% organoclay are prepared through the melt compounding process [11]. Both unfilled

nylon 6 and nylon 6–clay nanocomposite pellets purchased from RTP Company were dried in a vacuum oven at 90°C for 8 h to eliminate the moisture content, if any, and then injection molded into the cylindrical specimens (10 mm long and 10 mm diameter) for compression tests. The barrel temperatures in the injection molding machine were 245, 260, and 255°C from hopper to die, and the mold temperature was 120°C. The injection pressure and the holding pressure were 11.27 and 13.72 MPa, respectively. All specimens were polished using a lapping machine with 25 μm aluminum oxide powder to ensure smooth and flat loading surfaces.

It is to be noted that since nylon 6 is hygroscopic, even nylon 6–clay is prone to absorb moisture well and the corresponding mechanical properties could be affected dramatically by the moisture content. As a result, two environmental conditions, i.e., dry condition and wet condition were accounted for in the preparation of the specimens. For dry condition, the specimens were kept in a vacuum oven at a temperature of 45°C to prevent any moisture absorption. However, for wet condition, the specimens were immersed in water kept at 45°C for 20 days to accelerate the moisture absorption. The moisture content (wt%) was recorded daily and the results are shown in Figure 1. It is shown that after twenty days, the moisture contents were almost saturated and unfilled nylon 6 specimens absorbed more water than the nylon 6–clay nanocomposite specimens, which illustrates that the presence of organoclay retards water absorption capacity of the nylon 6.

The degree of exfoliation and dispersion of the organoclay in the nanocomposites were evaluated by X-ray diffraction (XRD) and transmission electron microscope (TEM). For XRD examination, the neat nylon 6 and nylon 6–clay nanocomposite films with 0.8 mm thickness and 10 mm diameter were fabricated from the cylindrical specimen using precision section saw. The XRD measurement was conducted using a BEDED1 diffractometer with an X-ray wavelength of 1.54 Å at a scanning rate of 0.08°/s from 0.3 to 8°. Figure 2 shows the XRD patterns of the nylon 6–clay nanocomposites and the neat unfilled nylon 6 from which the *d*-spacing of the clay platelets in the nanocomposites was estimated as around 9 nm. For TEM analysis, samples of 100 nm thickness were

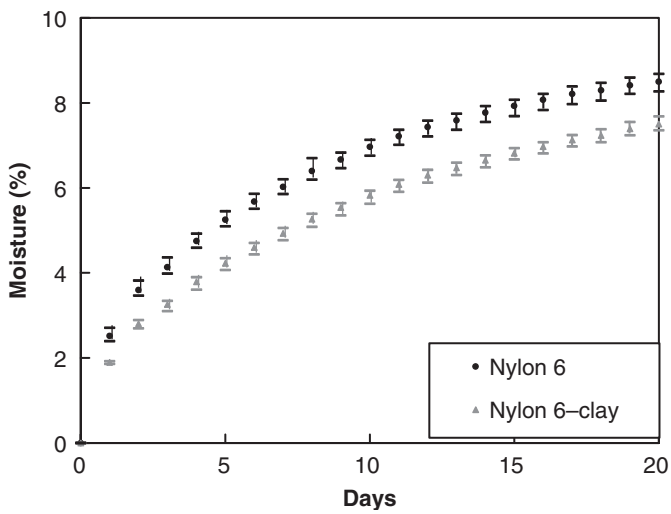

Figure 1. *The moisture content of wet nylon 6 and wet nylon 6–clay nanocomposites.*

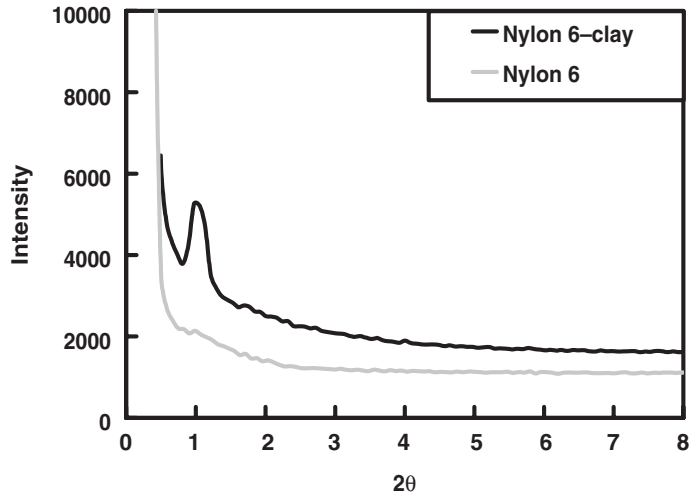

Figure 2. *The X-ray diffraction patterns of neat nylon 6 and nylon 6–clay nanocomposites.*

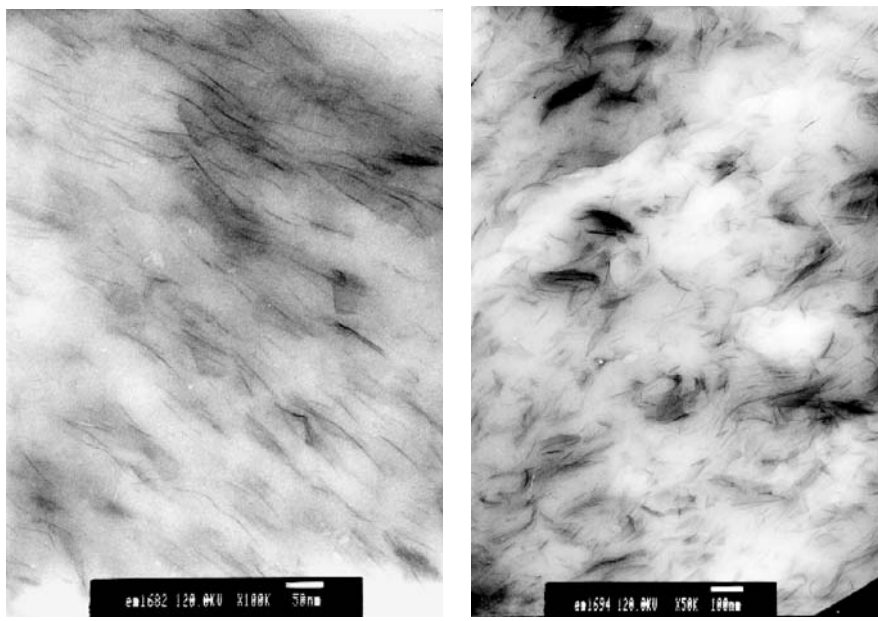

(a) (b)

Figure 3. *TEM micrographs of nylon 6–clay nanocomposites: (a) 100,000 and (b) 50,000.*

prepared using a microtome in cryogenic conditions. The TEM observations of nylon 6–clay nanocomposites were carried out by a JEOL 200CX with an acceleration voltage of 120 KV. The micrographs with 100,000 and 50,000 magnifications are illustrated, respectively, in Figure 3. The figure shows that most of the platelets distributed in the matrix are in the form of intercalated clusters and the interlayer spacing is around 7–9 nm

which is compatible with the results of XRD. Moreover, there are some layers of platelets locally exfoliated and randomly dispersed in the sample. As a result, the material investigated in this study is a combination of intercalated and partially exfoliated nanocomposites.

EXPERIMENTAL PROCEDURE

To investigate the strain rate effect, nylon 6–clay nanocomposites were tested in compression at various strain rates. High strain-rate experiments were conducted using the SHPB. However, for low strain rates, the tests were carried out on the hydraulic MTS machine.

High Strain Rate Tests

High strain rate compression tests were performed on nylon 6 and nylon 6–clay nanocomposites using the SHPB, which is an effective but simple apparatus for establishing the dynamic constitutive relations [12]. Figure 4 demonstrates a typical two-gage configuration of a SHPB, where gage A measures both the incident and the reflected pulses in the incident bar, while gage B measures the transmitted pulse. At each of these locations, a pair of diametrically opposed gages were mounted to compensate the bending effect that resulted from the eccentric impact of the striker bar on the incident bar. The SHPB setup used in this study was made of hardened steel bars with a diameter of 13.3 mm. The striker bar had a length of about 90 mm, and the incident bar and the transmission bar were 91 and 56 cm long, respectively. During the tests, the strain-gaged cylindrical specimen was sandwiched between the incident bar and the transmission bar. While the impact pulse propagates along the pressure bars and the specimens, the corresponding strain signals measured from the gages were converted into voltage signals by Wheatstone bridge circuits and then amplified using conditioning amplifier. Finally, the signals were recorded by the digital oscilloscope with a sampling rate of 10 MHz.

It is to be noted that there are two different bar systems, i.e., steel bar and aluminum alloy (6061-T6) bar, employed for the high strain rate tests. The selection of the bar system is based on the relative magnitudes of the pulse signals propagating on the transmission bar to the surrounding noise. For dry nylon 6 and nylon 6–clay samples, since the amplitudes of the gage signals on the steel transmission bars are high enough to be recognized, the experiments were conducted using a steel SPHB. On the other hand, for the wet specimens with lower mechanical impedances, the transmitted gage signals on the

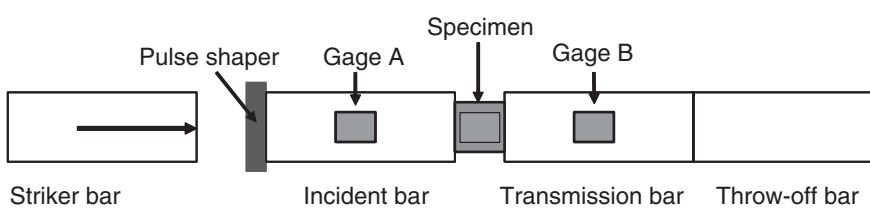

Figure 4. *The split Hopkinson pressure bar apparatus.*

steel bars are so weak that the noise prevents the proper interpretation of the measured signals. Therefore, to effectively enhance the amplitude of the gage signals on the bars, an aluminum alloy SHPB [8] with the characteristic of lower stiffness was employed instead of steel SHPB for testing the wet samples. A pulse-shaper technique was utilized to produce a gently rising loading pulse which would facilitate the stress equilibrium and homogeneous deformation of the specimens during the high strain rate tests. As a result, reliable stress and strain curves, especially in the small strain range, can be extracted from the SHPB tests [13,14]. This pulse shaping can be achieved using a piece of soft material inserted between the striker bar and the incident bar. In this study, 3 mm thick copper and 5 mm thick nylon 6 disks were selected as a pulse shaper for steel and aluminum bar systems, respectively.

The typical strain gage signals measured from the incident, transmission bars and the specimen, respectively, of dry nylon 6–clay nanocomposites are shown in Figure 5. The excitation voltages of the Wheatstone bridge circuits for the gages on the bars and for the specimen gage were 5 and 3 V, respectively, and the corresponding amplifications were set to be 1000 for the gages on the bars and 25 for the specimen gage. Using the Hopkinson bar theory [12], the contact stress P_1 between the incident bar and the specimen, and P_2, the contact stress between the specimen and the transmission bar, can be extracted from the recorded pulse data. The contact stresses P_1 and P_2 of the dry nylon 6–clay nanocomposite specimen is shown in Figure 6. It is to be noted that P_1 and P_2 almost coincide with each other except that P_1 exhibits greater oscillations than P_2. Hence, we took P_2 to calculate the compressive stress in the specimen to generate the dynamic stress–strain curve.

Conventionally, the strain history of the specimen during loading can also be calculated using the Hopkinson bar formula with expressions of displacements at the ends of the bars derived from the strain responses recorded at gage A and gage B [12]. In the present study, the strain response of the specimen was also measured using strain gage directly mounted on the specimen. Figure 7 shows the comparison of the strain histories for the nanocomposite specimen obtained using the Hopkinson bar formula and the strain gage

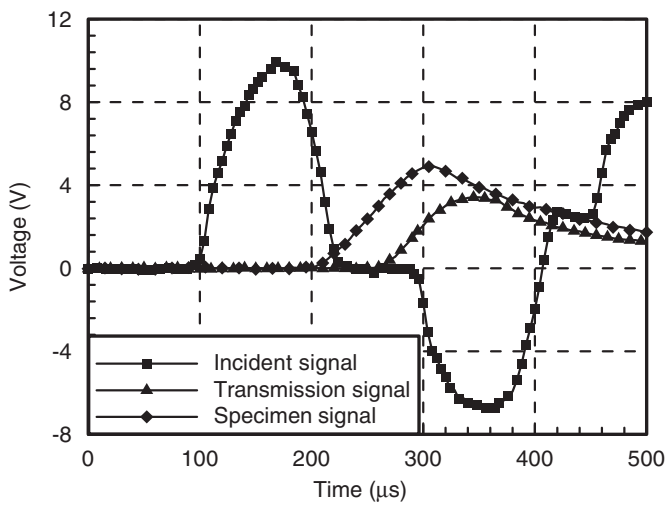

Figure 5. *Strain gage signals recorded in the SHPB test of dry nylon 6–clay nanocomposites.*

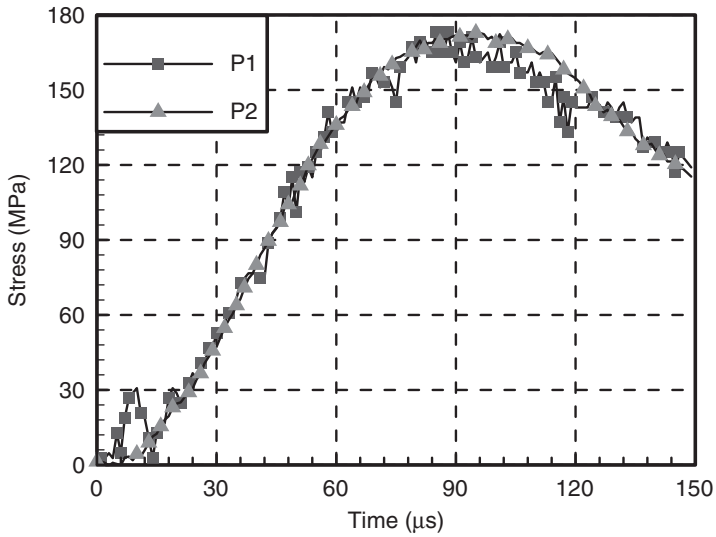

Figure 6. *Time histories of the contact stresses of dry nylon 6–clay nanocomposites in the SHPB tests.*

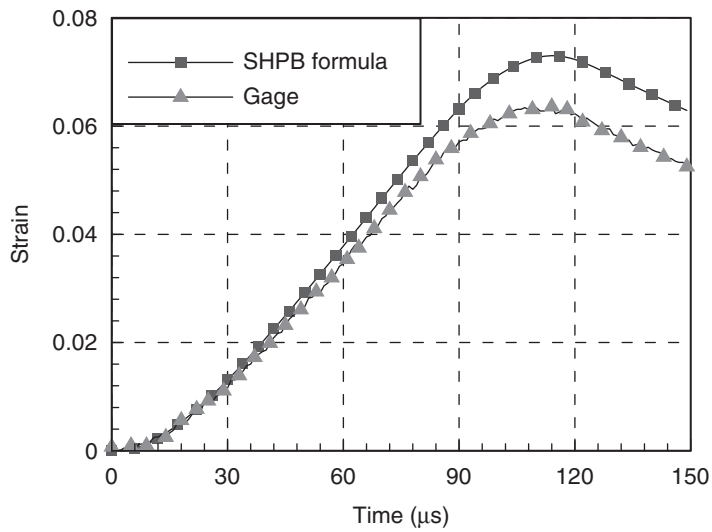

Figure 7. *Strain history obtained from the Hopkinson bar formula and the specimen gage signal for dry nylon 6–clay nanocomposites in the SHPB tests.*

directly mounted on the specimen, respectively. It is evident that the strain history calculated based on the Hopkinson bar theory deviates from that directly measured from the specimen. In this study, the strain history directly measured from the specimen was adopted for the determination of the strain rate and for the generation of the dynamic stress–strain curves as well. The average strain rate measured in the steel SHPB tests was 800/s. Similarly, the high strain rate experiments were performed on the wet specimens using an aluminum alloy SHPB. The stress curves were calculated based on the contact

stress between the specimen and the transmission bar and the corresponding strain curve was obtained from the strain gage adhered on the specimen. The average strain rate in the aluminum SHPB test for the wet samples was around 500/s.

Low Strain Rate Tests

For strain rates less than 1/s, the compression tests were performed on nylon 6 and nylon 6–clay nanocomposites using the hydraulic MTS machine. The uniaxial compressive loading was applied on the cylindrical specimens through the end surfaces, as shown in Figure 8. For consistency, the samples used for the low strain rate tests were the same as those in the SHPB tests. A self-adjusting device was applied to eliminate potential bending moments and also to ensure the specimen to be in full contact with the loading surfaces. During the tests, the contact surfaces of the specimens and the loading fixture were lubricated to reduce the contact friction (Figure 8).

Two different nominal strain rates of 0.0001/s and 0.1/s were performed at stroke control mode. The nominal strain rate is the stroke rate of the loading frame divided by the original specimen length. The corresponding true strain rates were measured using strain gages directly mounted on the specimens. The applied load, displacement, and gage signals for each test were recorded using LabVIEW. Figure 9 shows the nominal strain curve and the true strain curve for a dry nylon 6–clay specimen tested at the nominal strain rate of 0.0001/s. It is evident that the true strain curve is quite different from the nominal strain curve and thus the true strain rate is also different from the nominal strain rate. This discrepancy could be ascribed to the use of the self-adjusting device (Figure 8) for the compression test. In this study, the true strain curve was adopted for the generation of the stress and strain curves and for the calculation of the axial strain rate as well. For the experiments conducted at the nominal strain rate of 0.0001/s, the average true strain rate measured was 8×10^{-5}/s. In addition, the average true strain rate was 8×10^{-2}/s corresponding to the tests at the nominal strain rate of 0.1/s.

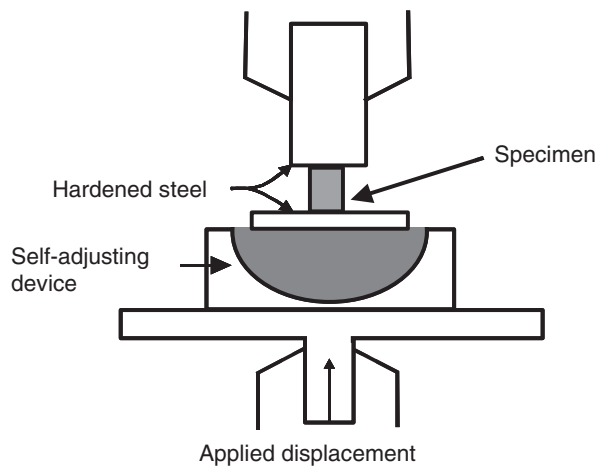

Figure 8. *Apparatus for low strain rate tests.*

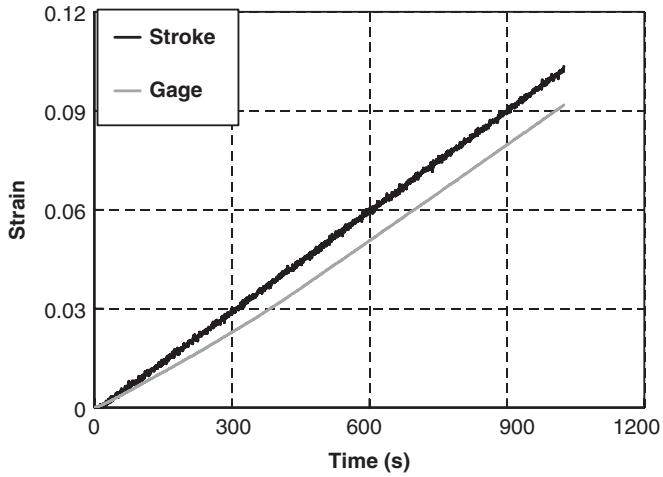

Figure 9. *Strain history obtained from stroke and strain gage of dry nylon 6–clay nanocomposites at a nominal strain rate of 0.0001/s.*

RESULTS AND DISCUSSION

Strain Rate Effect

The stress and strain curves of the dry nylon 6–clay nanocomposites at true strain rate ranges from 8×10^{-5} to 800/s are shown in Figure 10. The constitutive relations exhibit an apparently linear elastic range followed by nearly perfect plastic behavior. It is shown that the slopes of the linear portions are almost the same within the strain rate ranges tested, which indicates that the Young's modulus of the dry nanocomposites is not affected apparently by the strain rates. The Young's modulus for the dry nylon 6–clay nanocomposites measured is around 4.1 GPa. However, the linear elastic ranges of the stress and strain curves increase when the strain rate increases.

The stress and strain curves of wet nylon 6–clay nanocomposites at three different strain rates, 8×10^{-5}, 8×10^{-2}, and 500/s are shown in Figure 11. It is shown that for the wet samples, the constitutive curves are almost nonlinear except at the strain rate of 500/s. The stiffening behavior becomes more significant as the strain rate increases. Theoretically, the Young's modulus of the material should be determined from the initial slope of the stress and strain curves. However, due to the nonlinearity, it becomes a challenging task to decide a suitable initial strain range for the evaluation of the Young's modulus. In this study, for a true strain rate up to 0.08/s, the experimental data within a strain range of 0.2% was selected for the determination of the Young's modulus of the nanocomposites. If the initial strain range selected is too small, the corresponding experimental data will be scarce and scattering, which is not suitable for the correct interpretation of the Young's modulus. By curve-fitting the experimental data with a linear function, the corresponding value of the Young's modulus was evaluated as shown in Figure 12.

For high strain rate tests, the initial portions (strain $<0.5\%$) of the stress and strain curves are quite oscillating and inappropriate for the determination of the Young's modulus. However, the constitutive curves demonstrate an apparently larger linear range

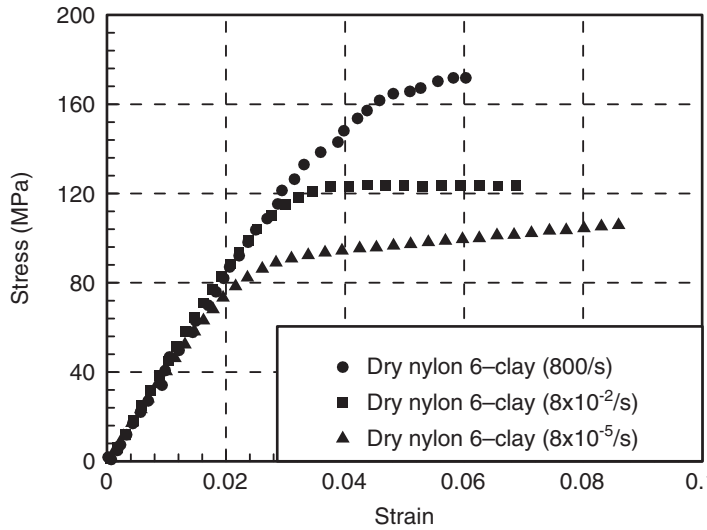

Figure 10. *Stress and strain curves of dry nylon 6–clay nanocomposites at three different strain rates.*

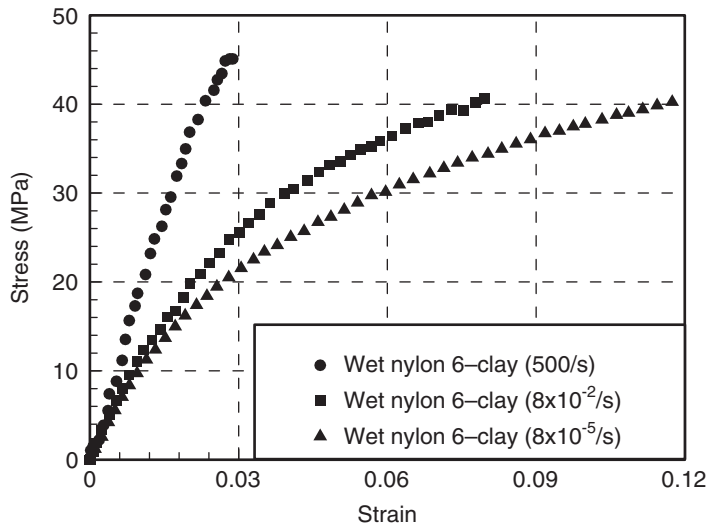

Figure 11. *Stress and strain curves of wet nylon 6–clay nanocomposites at three different strain rates.*

than those in the lower strain rate tests. Thus, we resort to the stress and strain data with the strain level up to 0.5% for evaluating the Young's modulus. Again, a linear function was employed to fit these experimental data and the results are shown in Figure 13. The Young's modulus determined by the above-mentioned procedures is summarized in Table 1. It can be seen that for wet nylon 6–clay nanocomposites, the Young's modulus increases with the increment of the strain rate, which is contrary to the dry nylon 6–clay

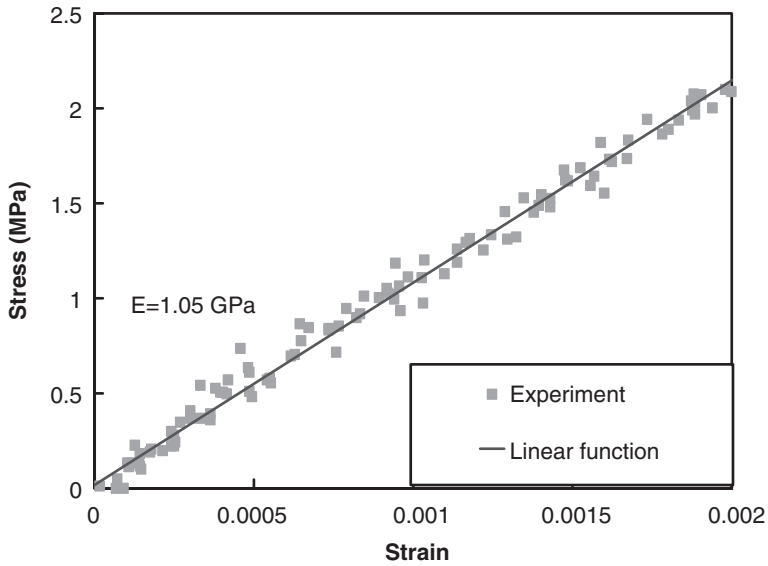

Figure 12. *Determination of Young's modulus of wet nylon 6–clay nanocomposites at a true strain rate of* 8×10^{-5}*/s.*

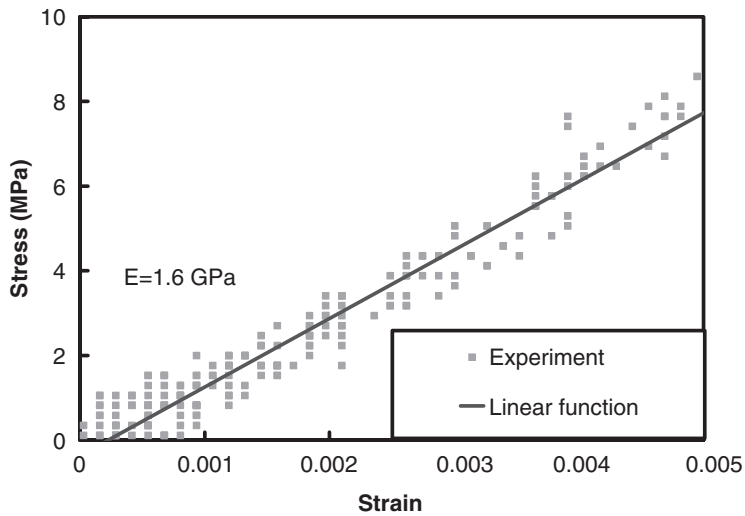

Figure 13. *Determination of Young's modulus of wet nylon 6–clay nanocomposites at strain rate of 500/s.*

nanocomposites. In addition, for each strain rate, the wet nylon 6–clay nanocomposites always demonstrate inferior mechanical response, such as stiffness and yielding stress than the dry ones. Therefore, it should be of concern that the rate dependency as well as the corresponding mechanical properties of nylon 6–clay nanocomposites would be affected dramatically by the moisture absorption.

Table1. Young's modulus of wet nylon 6 and nylon 6–clay nanocomposites at three different strain rates.

Material	High (500/s)	Intermediate (8×10^{-2}/s)	Low (8×10^{-5}/s)
Nylon 6 (moisture)	1.2 GPa (8.27%)	1.0 GPa (8.52%)	0.73 GPa (8.49%)
Nylon 6–clay nanocomposite (moisture)	1.6 GPa (7.48%)	1.24 GPa (7.64%)	1.05 GPa (7.65%)
Enhancement ratio (%)	33%	24%	43%

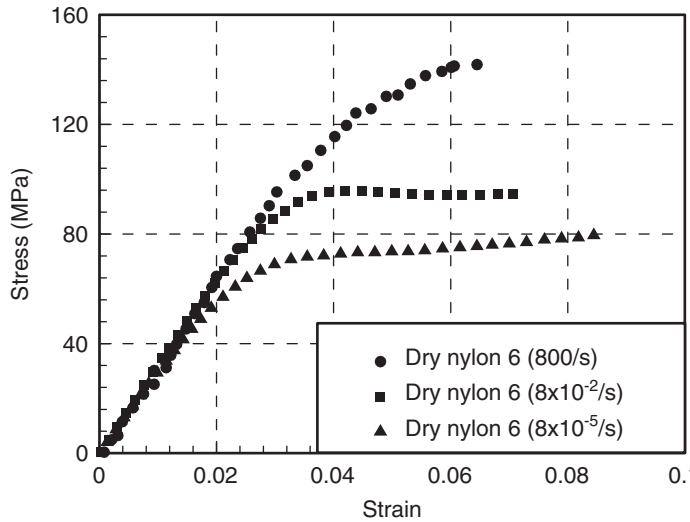

Figure 14. *Stress and strain curves of unfilled dry nylon 6 specimens at three different strain rates.*

Organoclay Effect

To examine the effect of organoclay on the mechanical responses of the nylon 6 nanocomposites, the unfilled nylon 6 was also tested in the same manner. Figure 14 shows the stress and strain curves of unfilled dry nylon 6 at different strain rates. The constitutive behavior of the unfilled dry nylon 6 is quite similar to those in dry nylon 6–clay nanocomposites except that the yielding stress and the Young's modulus are lower. From the quantitative comparison, it is revealed that the supplement of 5 wt% organoclay in the dry nylon 6 can enhance the Young's modulus up to 32%.

The experimental results for the unfilled wet nylon 6 samples are illustrated in Figure 15, and again by following the same procedure described earlier, the corresponding Young's modulus was determined. The results are also summarized in Table 1. Similar to the dry samples, the wet nylon 6–clay nanocomposites exhibit higher stiffness than the wet nylon 6. Moreover, the enhancement can be achieved up to 43% when the strain rate is 8×10^{-5}/s. It is interesting to mention that the enhancement ratio seems to be not affected significantly by the strain rate. This enhancement in the wet nylon 6–clay nanocomposites

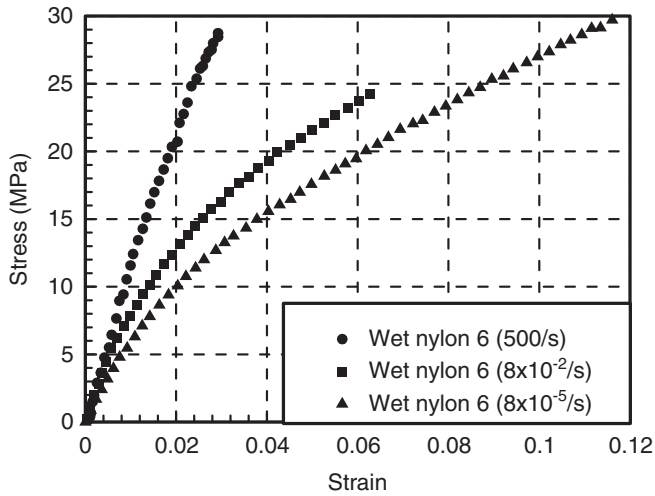

Figure 15. *Stress and strain curves of unfilled wet nylon 6 specimens at three different strain rates.*

can be attributed to the addition of the organoclay and its effect on the relative moisture content. For the wet unfilled nylon 6 and nylon 6–clay nanocomposites immersed in water for 20 days, the moisture contents are different. Apparently, the nylon 6–clay nanocomposites contain less moisture than nylon 6. As a result, the inclusion of the organoclay can retard the moisture absorption and effectively improve the stiffness of the wet nylon 6 in both linear and nonlinear ranges.

CONCLUSIONS

The following conclusions are obtained from the present study on the strain rate effect on the mechanical behavior of nylon 6–clay nanocomposites:

- For dry nylon 6–clay nanocomposites, the Young's modulus is not affected significantly by the strain rate at the strain rate up to 800/s. However, the linear elastic limit increases when the strain rate increases.
- For wet nylon 6–clay nanocomposites, the constitutive curves are almost nonlinear and the Young's modulus increases with the increase of strain rate. In addition, moisture content dramatically reduces the stiffness of nylon 6–clay nanocomposites and significantly affects the rate sensitivity of the Young's modulus of the nylon 6–clay nanocomposites.
- The supplement of 5 wt% organoclay in the dry nylon 6 can enhance the Young's modulus to 32% within the tested strain rate ranges. Moreover, the enhancement can be up to 43% in the wet nylon 6 samples.

ACKNOWLEDGMENTS

This study was supported by the National Science Council, Taiwan under the contract No. NSC 92-2212-E-009-029 to National Chiao Tung University.

REFERENCES

1. Pinnavaia, T.J. and Beall, G.W. (2000). *Polymer-Clay Nanocomposites*, John Wiley & Sons Ltd, New York.
2. Usuki, A., Kojima, Y., Kawasumi, M., Okada, A., Fukushima, Y., Kurauchi, T. and Kamigaito, O. (1993). Synthesis of Nylon 6-Clay Hybrid, *Journal of Materials Research*, **8**(5): 1179–1184.
3. Cho, J.W. and Paul, D.R. (2001). Nylon 6 Nanocomposites by Melt Compounding, *Polymer*, **42**(3): 1083–1094.
4. Dennis, H.R., Hunter, D.L., Chang, D., Kim, S., White, J.L., Cho, J.W. and Paul, D.R. (2001). Effect of Melt Processing Conditions on the Extent of Exfoliation in Organoclay-Based Nanocomposites, *Polymer*, **42**(23): 9513–9522.
5. Usuki, A., Koiwai, A., Kojima, Y., Kawasumi, M., Okada, A., Kurauchi, T. and Kamigaito, O. (1995). Interaction of Nylon 6-Clay Surface and Mechanical Properties of Nylon 6-Clay Hybrid, *Journal of Applied Polymer Science*, **55**(1): 119–123.
6. Kojima, Y., Usuki, A., Kawasumi, M., Okada, A., Kurauchi, T., Kamigaito, O. and Kaji, K. (1994). Fine Structure of Nylon 6-Clay Hybrid, *Journal of Polymer Science: Part B: Polymer Physics*, **32**(4): 625–630.
7. Liu, L., Qi, Z. and Zhu, X. (1999). Studies on Nylon 6/Clay Nanocomposites by Melt-Intercalation Process, *Journal of Applied Polymer Science*, **71**(7): 1133–1138.
8. Tsai, J. and Sun, C.T. (2004). Effect of Platelet Dispersion on the Load Transfer Efficiency in Nanoclay Composites, *Journal of Composite Materials*, **38**(7): 567–579.
9. Chen, W., Lu, F. and Cheng, M. (2002). Tension and Compression Tests of Two Polymers under Quasi-Static and Dynamic Loading, *Polymer Testing*, **21**(2): 113–121.
10. Walley, S.M., Field, J.E., Pope, P.H. and Safford, N.A. (1989). A Study of the Rapid Deformation Behavior of a Range of Polymers, *Philosophical Transactions of the Royal Society of London A*, **328**(1597): 1–33.
11. RTP® Material Data Sheet.
12. Graff, K.F. (1975). *Wave Motion in Elastic Solids*, Dover Publications, New York.
13. Tsai, J. and Sun, C.T. (2002). Constitutive Model for High Strain Rate Response of Polymeric Composites, *Composites Science and Technology*, **62**(10–11): 1289–1297.
14. Chen, W., Song, B., Frew, D.J. and Forrestal, M.J. (2003). Dynamic Small Strain Measurements of a Metal Specimen with a Split Hopkinson Pressure Bar, *Experimental Mechanics*, **43**(1): 20–23.